JPE 17-2-8

https://doi.org/10.6113/JPE.2017.17.2.389
ISSN(Print): 1598-2092 / ISSN(Online): 2093-4718

Load Disturbance Compensation for Stand-alone Inverters Using an Inductor Current Observer

Jung-Muk Choe*, Seungryul Moon*, Byeng-Joo Byen**, Jih-Sheng Lai*, Young-Bae Lim***, and Gyu-Ha Choe†

*Future Energy Electronics Center, Virginia Tech, Blacksburg, VA, U.S.A
**,†Department of Electrical Engineering, Konkuk University, Seoul, Korea
***Korea Electrical Safety Corporation, Seoul, Korea

Abstract

A control scheme for stand-alone inverters that utilizes an inductor current observer (ICO) is proposed. The proposed method measures disturbance load currents using a current sensor and it estimates the inductor current using the ICO. The filter parameter mismatch effect is analyzed to confirm the ICO's controllability. The ICO and controllers are designed in a continuous-time domain and transferred to a discrete-time domain with a digital delay. Experimental results demonstrate the effectiveness of the ICO using a 5-kVA single-phase stand-alone inverter prototype. The experimental results demonstrate that the observed current matches the actual current and that the proposed method can archive a less than 2.4% total harmonic distortion (THD) sinusoidal output waveform under nonlinear load conditions.

Key words: Inductor current observer, Isolated grid, Load disturbance compensation, Single-phase inverter, Stand-alone inverter

NOMENCLATURE

Symbols

G	Transfer function
^	Estimated variable.

Subscripts (Used Singly or in Combination)

L	Inductor
C	Capacitor
c	Controller.

I. INTRODUCTION

Stand-alone type inverters are widely used to supply electrical power to places with isolated grid connections [1]-[5]. The goal of a stand-alone inverter is to maintain a sinusoidal output voltage with a low total harmonic distortion (THD) and fast transient dynamics. Recently, nonlinear residential electrical loads have dramatically increased because of the introduction of electronic loads, leading to problems such as voltage variations and waveform distortion. These problems can result in steady-state errors and distortions in the supply voltage waveform in stand-alone type inverters.

The structure of a typical inverter's output voltage controller comprises multiple feedback loops rather than a single feedback loop [6], [7]. A multiple feedback loop controller is typically composed of an outer voltage control loop and an inner current control loop. Numerous control strategies such as predictive control [8], dead-beat control [9]-[11], and repetitive control [12] have been used for controlling the outer and inner loops to ensure a good output quality. The current controller attenuates the effects of disturbances in the load and contributes to the stability of the voltage control loop [13]-[19]. The current control loop can control either the inductor current or the capacitor current. Excellent results using a capacitor current control have been reported in several papers [19], [20]. One of the drawback to using capacitor current feedback is the tremendous amount of switching noise that can render the current feedback unusable [21]. In addition, overcurrent protection is not possible because there is no information on the inductor or load current, which results in system unreliability. To overcome

Manuscript received Apr. 29, 2016; accepted Dec. 16, 2016
Recommended for publication by Associate Editor Sung-Jin Choi.
†Corresponding Author: ghchoe@konkuk.ac.kr
Tel: +82-2-450-3486, Fax: +82-2-450-1452, Konkuk University
*Future Energy Electronics Center, Virginia Tech, U.S.A
**Dept. of Electrical Eng., Konkuk University, Korea
***Korea Electrical Safety Corporation, Korea

© 2017 KIPE

these disadvantages, an inductor current feedback scheme with load current feedforward has been implemented by inserting two current sensors in the inductor and load [7], [13]. This scheme is identical to a capacitor current feedback scheme from the perspective of voltage regulation, and it protects the stand-alone inverters from overcurrent problem because it provides information on the inductor and load current. However, the load current feedforward scheme requires an additional current sensor for measuring the load current. As a result, the overall price of the system is increased. To overcome this limitation, a combined sensing has been proposed [20]. However, the bandwidth of this controller is limited by a low-pass filter.

In this study, to address the aforementioned disadvantages, an inductor current observer (ICO) feedback and a load current feedforward are proposed using a single current sensor. Compared to the existing method using two individual current sensors, the proposed method saves implementation costs and reduces the size of the system by reducing the number of required current sensors. Section II presents the system models of different current feedback schemes, and the ICO is proposed in Section III. Design guidelines are described in Section IV, and in Section V, experimental results demonstrate the favorable performance of the ICO. Finally, some concluding remarks are given in Section VI.

II. Development of the Equivalent Circuit Model

A. System Model in the Continuous-Time Domain

Single-phase full-bridge inverters are typified by the components shown in Fig. 1. The typical system is composed of four switches ($S_{1\sim4}$) and an output filter. The capacitor voltage (v_o) and the load current (i_o) are measured by sensors. The inductor current (i_L) information is obtained with the proposed inductor current observer. From i_o and i_L, the capacitor current (i_C) is constructed. The inductance of the output filter and its equivalent series resistance (ESR) are L and R_L, respectively, and the capacitor and an unknown load impedance are C and R, respectively. The capacitor ESR is ignored because the cutoff frequency appears far above the Nyquist frequency.

A continuous-time state-space model of the above figure can be generally expressed as follows:

$$\dot{x}(t) = Ax(t) + Bu(t) \tag{1a}$$

$$y(t) = Cx(t) \tag{1b}$$

$$\begin{bmatrix} \dot{v}_o(t) \\ \dot{i}_L(t) \end{bmatrix} = \begin{bmatrix} 0 & \frac{1}{C} \\ \frac{-1}{L} & \frac{-R_L}{L} \end{bmatrix} \begin{bmatrix} v_o(t) \\ i_L(t) \end{bmatrix} + \begin{bmatrix} 0 & -\frac{1}{C} \\ \frac{1}{L} & 0 \end{bmatrix} \begin{bmatrix} v_{in}(t) \\ i_o(t) \end{bmatrix} \tag{1c}$$

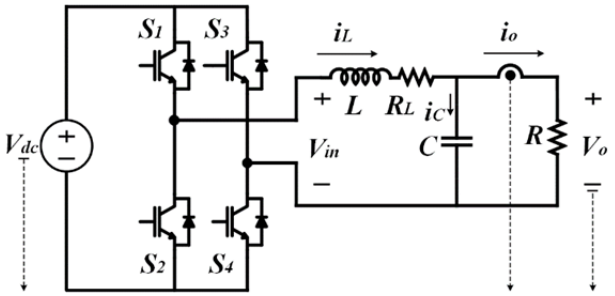

Fig. 1. Schematic of single-phase stand-alone inverter.

$$v_o(t) = \begin{bmatrix} 1 & 0 \end{bmatrix} \begin{bmatrix} v_o(t) \\ i_L(t) \end{bmatrix}. \tag{1d}$$

In (1a)–(1d), V_{in} is the averaged modulated voltage, which is a reference for the output voltage before the LC filter. The inductor current is the sum of the capacitor current and the load current as in (2):

$$i_L(t) = i_C(t) + i_o(t). \tag{2}$$

Equation (2) can be plugged in the second equation in (1) to yield:

$$\frac{d}{dt} i_C(t) + \frac{d}{dt} i_o(t) = -\frac{1}{L} v_o(t) - \frac{R_L}{L} \{ i_C(t) + i_o(t) \} + \frac{1}{L} v_{in}(t). \tag{3}$$

In (3), the differential load current can be alternately expressed in terms of the output voltage and the capacitor current as (4):

$$\frac{d}{dt} i_o(t) = \frac{1}{R} \frac{d}{dt} v_o(t) = \frac{1}{R \cdot C} i_C(t). \tag{4}$$

Using (3) and (4), the state equation of the capacitor current-controlled inverter in a continuous-time model can be expressed in the following matrix form:

$$\begin{bmatrix} \dot{v}_o(t) \\ \dot{i}_C(t) \end{bmatrix} = \begin{bmatrix} 0 & 1/C \\ -\frac{R_L}{R \cdot L} - \frac{1}{L} & -\frac{1}{R \cdot C} - \frac{R_L}{L} \end{bmatrix} \begin{bmatrix} v_o(t) \\ i_C(t) \end{bmatrix} + \begin{bmatrix} 0 \\ \frac{1}{L} \end{bmatrix} v_{in}(t) \tag{5a}$$

$$v_o(t) = \begin{bmatrix} 1 & 0 \end{bmatrix} \begin{bmatrix} v_o(t) \\ i_C(t) \end{bmatrix}. \tag{5b}$$

B. Analysis of the Current Feedback Methods in a Digital Model

To analyze the characteristics of the effect of the load current feedforward, a function is needed to describe the frequency response of the modulated voltage to the current transfer. Using (5), the capacitor current control transfer function $G_{i_C v}(s)$ can be obtained for the load current feedforward as in (6):

$$G_{i_C v}(s) = \frac{i_C(s)}{v_{in}(s)} = \frac{sCR}{s^2 LCR + s(L + CR_L R) + R_L + R}. \tag{6}$$

In (6), $G_{i_C v}(s)$ is the modulated voltage to the capacitor current transfer function. This system model is constructed in

TABLE I
PARAMETERS FOR THE INVERTER

Symbol	Value
Inductor (L)	583 μH
Capacitor (C)	13.3 μF
Inductor resistance (R_L)	0.3 Ω
Output Voltage (V_o)	200 V_{rms}
Frequency (f_o)	60 Hz
Input Voltage(V_{dc})	380 V
Sampling time (T_s)	25 μs
Sampling frequency (f_s)	40 kHz
Switching frequency (f_{sw})	40 kHz

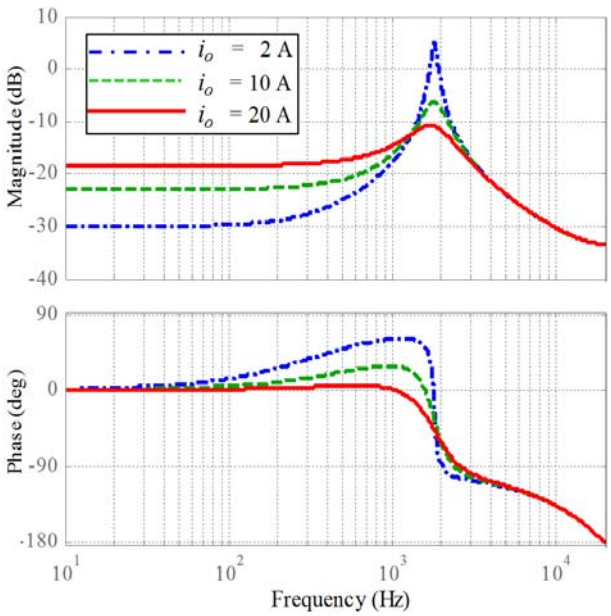

Fig. 2. Bode plot $G_{i_Lv}(s)$ of the inductor current control model (without i_o feedforward).

the continuous-time domain. It can be converted to the discrete domain using a z-transformation, incurring an additional delay. The computational delay from the iteration of the software routine in a digital controller is modeled as z^{-1}, as shown in Fig. 5. The inverter parameters shown in Table I are utilized for this numerical analysis. Fig. 2 shows a Bode plot of the modulated voltage to the inductor current transfer function, and Fig. 3 shows a Bode plot of the modulated voltage to the capacitor current transfer function, which uses the inductor current feedback and load current feedforward. Different output current i_o conditions were simulated by varying the load resistor R. These Bode plots illustrate the error difference that occurs under nonlinear load conditions. Nonlinear loads such as a rectifier load can be simply visualized as load steps between the no load and full load conditions as the rectifier diodes conducts. The target of the proposed current controller bandwidth is 3 kHz. The magnitude and phase vary between 10 Hz and 3 kHz in the

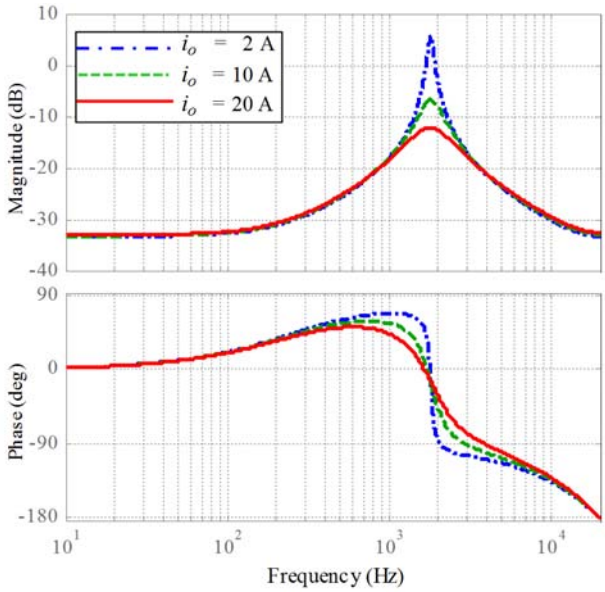

Fig. 3. Bode plot $G_{i_Cv}(s)$ of the capacitor current control model (with i_o feedforward).

inductor current control model, which excludes the load current feedforward. Meanwhile, they are nearly the same in the capacitor current control model, which contains the load current feedforward for varying the magnitude of the load current. Therefore, the load current feedforward can compensate the load disturbance. In other words, the capacitor current control model is more independent of load impedance than the inductor current control model. As a result, the former is more suitable for the proposed controller design.

III. DEVELOPMENT OF THE ICO

A. Observability

Previous researchers used two current sensors for inductor feedback and load current feedforward [7]. Both currents must be known for advanced control performance, and monitoring one of them with an observer can reduce the number of required sensors. A system is said to be completely observable if knowledge of the control and output vector over a finite number of time samples completely determines the state vector [22]. Based on this theory, the proposed ICO is designed to obtain the current state vector. Fig. 4 shows a diagram of the ICO: the output vector is $\hat{v}_o$, the input vectors are v_o and i_L, and the control vectors are i_o and v_{in}.

B. ICO Design

After identifying the requisite vectors, a system matrix can be designed based on a second-order continuous-time model of the LC output filter as expressed in (1). From (1), the ICO model is manipulated by the following matrix form:

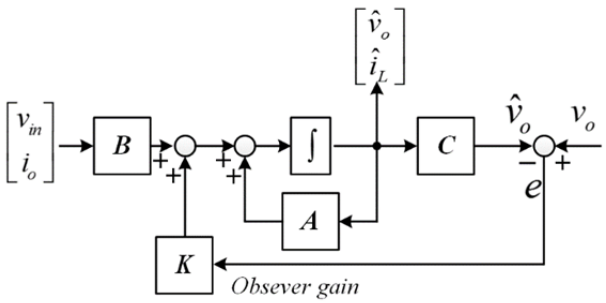

Fig. 4. Model of proposed ICO.

$$\dot{\hat{x}}(t) = A\hat{x}(t) + Bu(t) + K\left(\hat{y}(t) - y(t)\right) \tag{7a}$$

$$= A\hat{x}(t) + Bu(t) + K\left(C\hat{x}(t) - y(t)\right) \tag{7b}$$

$$\begin{bmatrix}\dot{\hat{v}}_o(t)\\ \dot{\hat{i}}_L(t)\end{bmatrix} = \begin{bmatrix}0 & \frac{1}{C}\\ \frac{-1}{L} & \frac{-R_L}{L}\end{bmatrix}\begin{bmatrix}\hat{v}_o(t)\\ \hat{i}_L(t)\end{bmatrix} + \begin{bmatrix}0 & -\frac{1}{C}\\ \frac{1}{L} & 0\end{bmatrix}\begin{bmatrix}v_{in}(t)\\ i_o(t)\end{bmatrix} + \begin{bmatrix}k_1\\ k_2\end{bmatrix}\left\{\begin{bmatrix}1 & 0\end{bmatrix}\begin{bmatrix}\hat{v}_o(t)\\ \hat{i}_L(t)\end{bmatrix} - y(t)\right\}. \tag{7c}$$

In (7), K is the matrix of the observer gain. The error dynamics are determined by subtracting the observer dynamics from the system dynamics, as in (8):

$$\dot{e}(t) = \dot{\hat{x}}(t) - \dot{x}(t) = \left(A - KC\right)\left(\hat{x}(t) - x(t)\right). \tag{8}$$

If the term $(A - KC)$ is stable, as indicated by having all of its eigenvalues in the left-half plane, the observer gain can be selected using eigenvalue assignment, as follows:

$$\det\left|\lambda I - (A - KC)\right| = \begin{bmatrix}s + k_1 & -\frac{1}{C}\\ k_2 + \frac{1}{L} & s + \frac{R_L}{L}\end{bmatrix} \tag{9a}$$

$$= s^2 + \left(k_1 + \frac{R_L}{L}\right)s + k_1\frac{R_L}{L} + \frac{k_2}{C} + \frac{1}{LC} = 0 \tag{9b}$$

$$2\varsigma\omega = k_1 + \frac{R_L}{L} \tag{9c}$$

$$\omega^2 = k_1\frac{R_L}{L} + \frac{k_2}{C} + \frac{1}{LC}. \tag{9d}$$

In (9), I is the 2 × 2 identity matrix. The observer gain K is given by (10), with ω as the angular crossover frequency and ς as the damping ratio:

$$K = \begin{bmatrix}k_1\\ k_2\end{bmatrix} = \begin{bmatrix}2\varsigma\omega - R_L/L\\ C\omega^2 - \left(2\varsigma\omega - \frac{R_L}{L}\right)\cdot\frac{CR_L}{L} - \frac{1}{L}\end{bmatrix}. \tag{10}$$

The continuous-time model of the ICO is to be regulated by a discrete-time controller with sampling and command updates at T_s. A zero-order hold (ZOH) at the controller output produces a piecewise constant command. The crossover frequency of the ICO is designed to be 3.5 kHz, and the damping ratio is 0.707. Using (10) and the parameters in Table I, the designed ICO's discrete equivalent model is written as follows:

$$\hat{x}(k+1) = \Phi\hat{x}(k) + \Gamma u(k) + K_T e(k), \tag{11}$$

where:

$$\Phi = e^{AT_s} = \begin{bmatrix}0.9608 & 1.8320\\ -0.0419 & 0.9566\end{bmatrix}, \tag{12a}$$

$$\Gamma = (e^{AT_s} - I)A^{-1}B = \begin{bmatrix}-0.9180 & 0.0196\\ 0.0196 & 0.0209\end{bmatrix}, \text{ and} \tag{12b}$$

$$K_T = (e^{AT_s} - I)A^{-1}K = \begin{bmatrix}0.4471\\ 0.0539\end{bmatrix}. \tag{12c}$$

C. Controller Design with the ICO

Fig. 5 shows a control block diagram of an inverter, with a double loop control strategy. The inner loop is a current control loop that uses information on two currents with one sensor. The inductor current feedback is constructed by the ICO, and the load disturbance is compensated by the load current feedforward. The outer loop is a voltage control loop.

In this study, the current controller is designed so that the targeted phase margin is 60º at the 3 kHz crossover frequency. D. Venable [23] introduced a K-factor design methodology that indicates the distance between the frequency position of the poles and zeros brought by a compensation network. Using the K-factor design, the current controller $G_{ic}(z)$ is given as follows:

$$G_{ic}(z) = \frac{2.991z^3 - 1.349z^2 - 2.766z + 1.575}{z^3 - 1.936z^2 + 1.155z - 0.219}. \tag{13}$$

The results obtained with this design are shown in Fig. 6, were the crossover frequency, indicating crossover frequency,

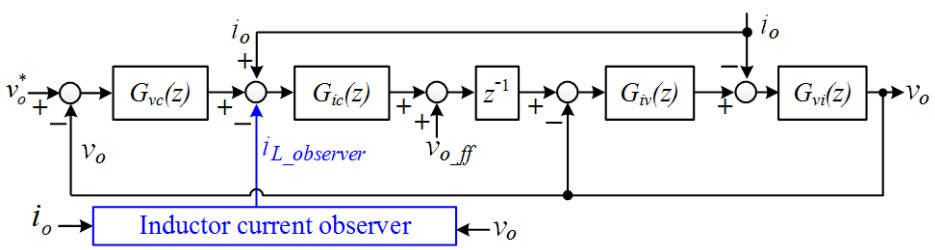

Fig. 5. Control block diagram of inverter with the ICO.

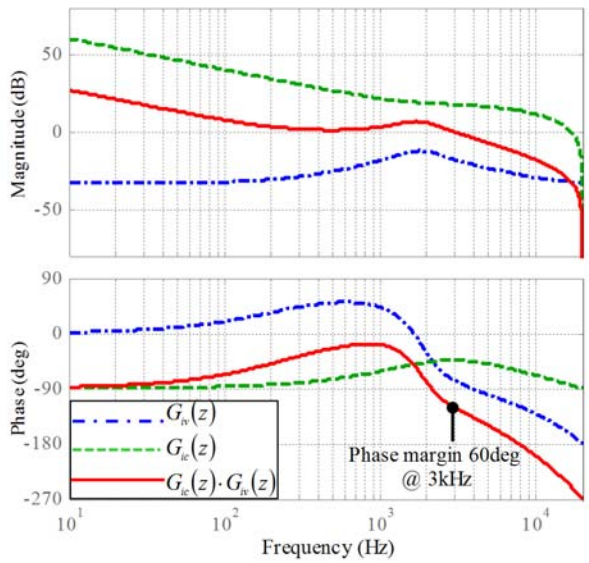

Fig. 6. Bode plot of the current control loop, with $G_{iv}(z)$ in blue, controller $G_{ic}(z)$ in green, and compensated gain $G_{ic}(z)\cdot G_{iv}(z)$ in red.

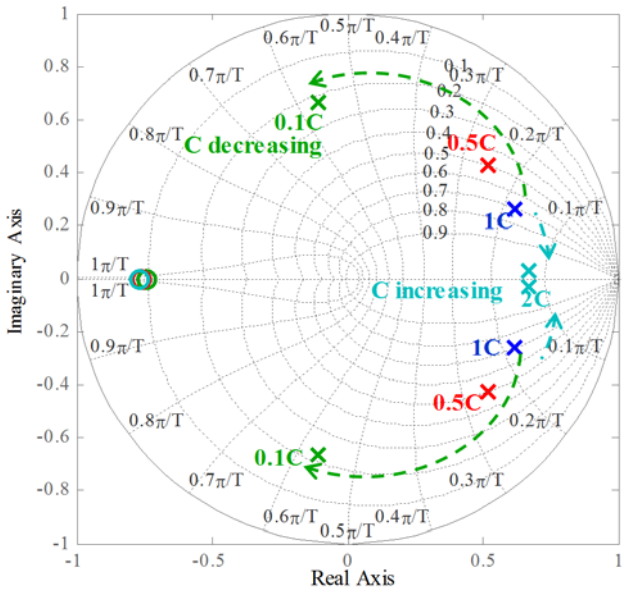

Fig. 7. ICO poles with variation in actual output capacitance.

and phase margin of the current control loop are shown in the design specifications. The magnitude is 4dB at 350Hz which is an aggressive design. Decreasing the resonant frequency of *LC* filter can make the current control loop more stable.

IV. Design Guidelines

A. Filter Capacitor Size and Material

The output filter plays an important role in rejecting switching noise. The cutoff frequency can be determined from the switching frequency. 20kHz is chosen for the design value. For a 40dB reduction 2nd order *LC* filter design, 2kHz is selected as the cutoff frequency, and *LC* can be calculated using characteristic impedance [24] as follows:

$$Z = \sqrt{\frac{L}{C}}\frac{240V}{\sqrt{2}\cdot 20.8A} = 8.5 \tag{14a}$$

$$f_{LC} = \frac{1}{2\pi\sqrt{LC}} = 2kHz \tag{14b}$$

$$L = 676\,uH\,,\ C = 10\,uF\,. \tag{14c}$$

A large capacitor can handle the capacitor voltage control and stabilize the output voltage under transient current conditions. However, a large filter size unfavorably reduces the system's power density. Furthermore, in practical applications, the dissipation factor (DF) at high frequencies should be considered. The DF is defined as the ratio of the ESR. Plastic film capacitors are much bigger than ceramic capacitors, but with a lower DF. Therefore, in this study, a polypropylene filter is selected as the best choice for high frequency applications among the plastic film capacitors. However, the small size of the filter can make it more challenging to implement the capacitor voltage control.

B. Parameter Mismatch Effect of the ICO

To confirm the sensitivity of the ICO to parameter mismatches, a controllability analysis is performed by mapping the eigenvalues of (9), in which the ICO poles are evaluated based on the nominal value. Fig. 7 illustrates the eigenvalue migration of the root locus, for a varied actual output capacitance C in the range of 0.1 times to 2 times the nominal capacitance. In Fig. 7, the closed-loop poles are located at 0.618 ± j0.261 with a 0.707 damping and a 3.5-kHz cross over frequency when C is the nominal value. However, the poles move in response to parameter variations. They are located at 0.67 ± j0.03 with 2 C, and at 0.106 ± j0.665 with 0.1 C. These results show that the damping ratio and the cross over frequency vary. The damping ratio is 0.23 at 0.1 C and it is 0.99 at 2 C. However, the closed-loop poles are located in a unit circle region, even with a variation in the actual output capacitance C from 0.1 to 2 C.

V. Experimental Procedure and Results

The proposed control scheme was tested in a 5-kVA single-phase inverter constructed for this purpose. Fig. 8 shows a picture of the experimental apparatus. A IGW40N65H5 IGBT manufactured by Infineon was chosen as the switch, and a TMS320F28335 manufactured by TI was used as the digital controller. For current sensing, a LA50-P manufactured by LEM with a bandwidth of 150 kHz was employed. The internal variables of the digital signal processor were displayed on an oscilloscope through a 12-bit digital-to-analog converter (DAC). Fig. 9 shows two types of nonlinear loads: (a) consists of a thyristor rectifier and a 26-Ω resistor, and (b) consists of a diode rectifier, a 160-Ω resistor, and a 502-μF capacitor.

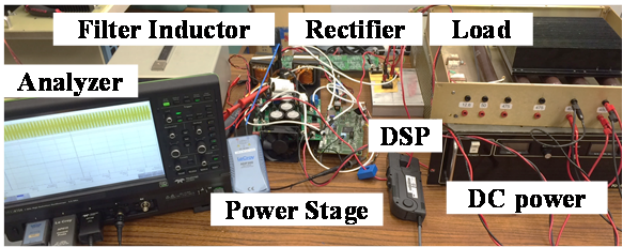

Fig. 8. Experimental apparatus.

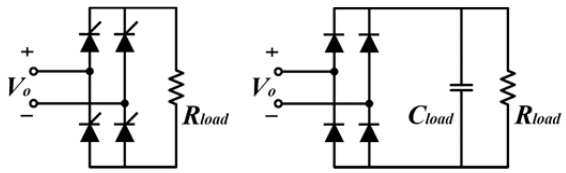

(a) (b)

Fig. 9. Two types of nonlinear load. (a) with a thyristor rectifier and resistor (R_{load} = 26 Ω), (b) with a diode rectifier, resistor, and capacitor (C_{load} = 502 uF, R_{load} = 160 Ω).

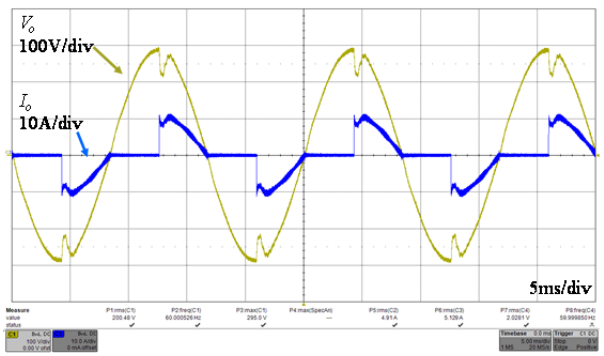

(a) Waveforms of output voltage and current.

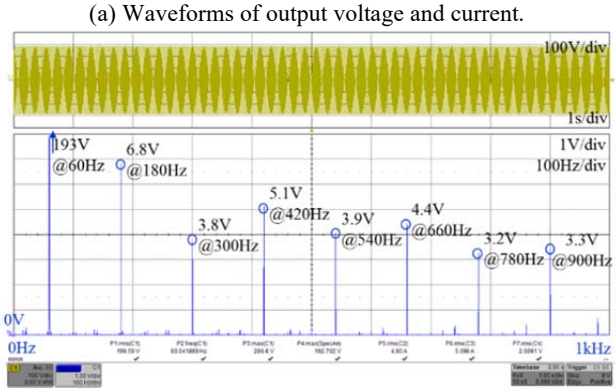

(b) Output voltage spectrum.

Fig. 10. Output voltage and current using the conventional method with thyristor rectifier load.

A. Thyristor Rectifier Load

Figs. 10 and 11 show the transient responses to incremental load disturbances using the thyristor rectifier load illustrated in Fig. 9(a). Fig. 10 shows the output voltage and current results using the conventional method, using the inductor current feedback without load current feedforward. The bandwidth of the current loop was set to 3 kHz with a 60° phase margin, and the bandwidth of the voltage loop was

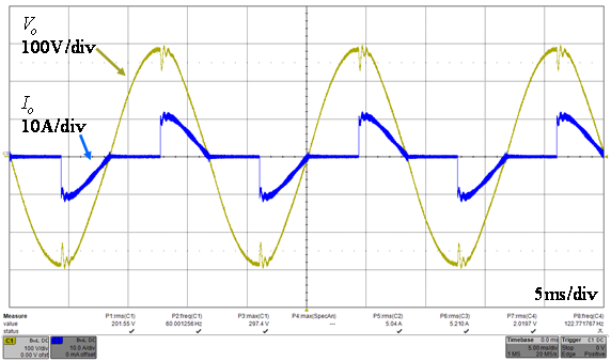

(a) Waveforms of output voltage and current.

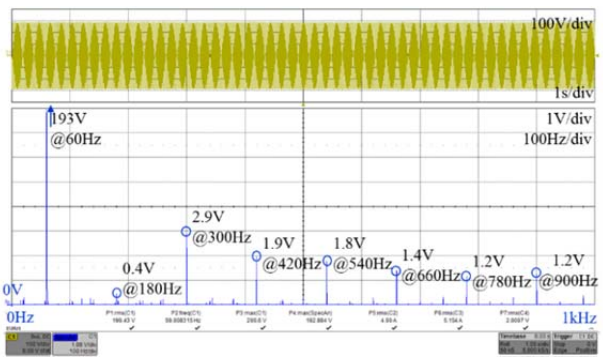

(b) Output voltage spectrum.

Fig. 11. Output voltage and current using the proposed method with thyristor rectifier load.

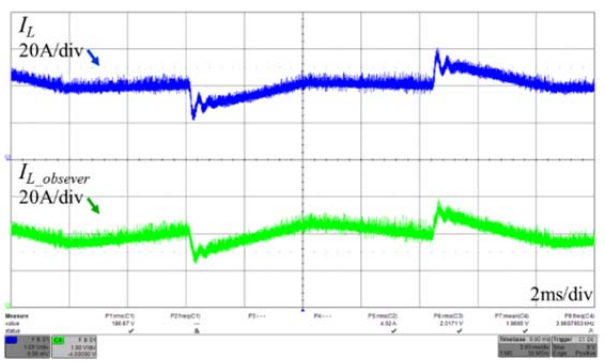

Fig. 12. Actual and observed currents with thyristor rectifier load.

set to 600 Hz with a 60° phase margin. As shown in Fig. 10(a), the output voltage and current do not immediately follow incremental changes in the load disturbance. Fig. 10(b) shows the output voltage spectrum. The third harmonic was 6.8 V, the fifth was 3.8 V, and the seventh was 5.1 V. The output voltage THD was 6.21 %. Fig. 11 shows the output voltage and current results using the proposed method, for which the voltage and current controller specifications were same as those for the conventional method. As shown in Fig. 11(a), the output performance was very good, and the load transient was recovered in approximately 0.4 ms. The third harmonic was 0.4 V, the fifth was 2.9 V, and the seventh was 2 V, as shown in Fig. 11(b). The output voltage THD was reduced to 2.35 %.

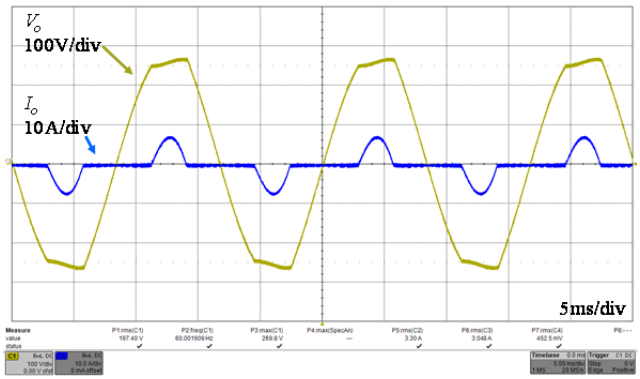

(a) Waveforms of output voltage and current.

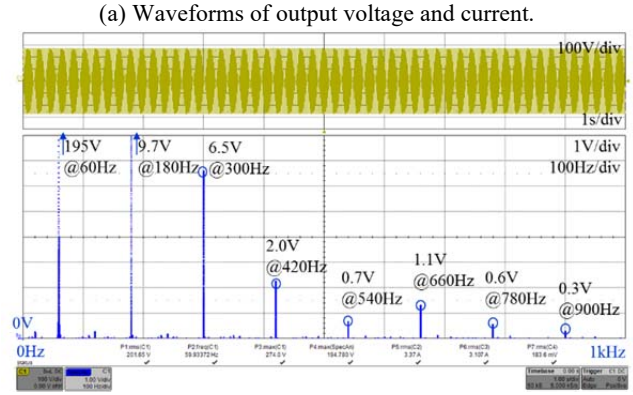

(b) Output voltage spectrum.

Fig. 13. Output voltage and current using the conventional method with diode rectifier load.

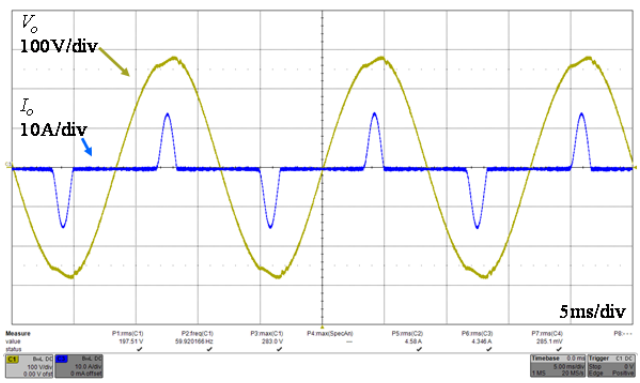

(a) Waveforms of output voltage and current.

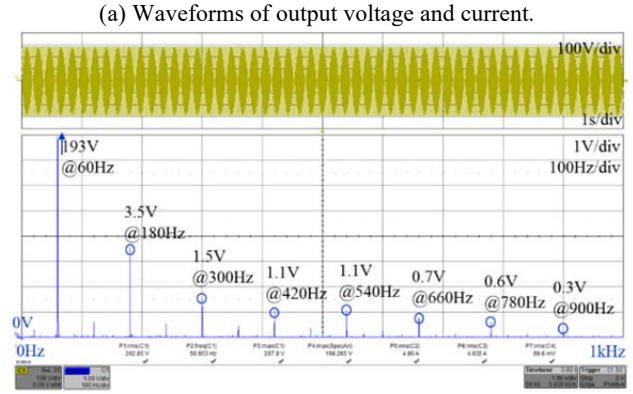

(b) Output voltage spectrum.

Fig. 14. Output voltage and current using the proposed method with diode rectifier load.

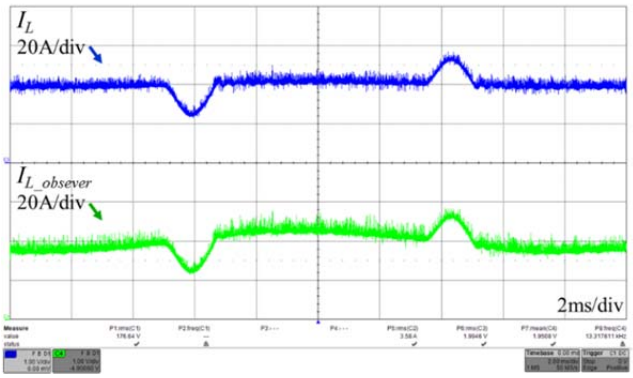

Fig. 15. Actual and observed currents with diode rectifier load.

Fig. 12 shows the result for the proposed ICO method, where I_L and $I_{L\_observer}$ were monitored using the DAC. The result shows the similarity between the actual current and that of the ICO.

B. Diode Rectifier Load

The output voltage and current results for the diode rectifier load in Fig. 9(b) are shown in Figs. 13, 14, and 15. As shown in Fig. 13(a), which illustrates the results for the conventional method, the output voltage was distorted by the load disturbance. The output voltage spectrum in Fig. 13(b) shows that the third harmonic was 9.7 V, the fifth was 6.5 V, and the seventh was 2.0 V. The output voltage THD was 6.14 %.

Fig. 14 illustrates the output voltage and current results for the proposed method, where the output voltage waveform exhibits a small deviation from an ideal sinusoidal waveform. The output voltage spectrum in Fig. 14(b) shows that the third harmonic was 3.54 V, the fifth was 1.52 V, and the seventh was 1.06 V. The output voltage THD was reduced to 2.2 %. Fig. 15 shows the results of the proposed method, where $I_{L\_observer}$ almost matches the actual current.

VI. CONCLUSION

This paper proposes an ICO for current controller feedback. The main purpose of using the ICO is as follows. First, by reducing the number of sensors, the system cost is reduced. Second, using the observed and measured current information, the load current feedforward is constructed, and load disturbances are compensated. This load current feedforward effect is validated by comparing the system model and experimental results. The ICO model is dependent on the *LC* filter parameter. However, the ICO was found to be controllable and observable for reasonable variations in the actual output capacitance. The THD values of the sinusoidal output are reduced below 2.4% even under conditions such as nonlinear loads and very low parameters of the LC filter, which verified the experimental results through the application of the proposed controller.

TABLE II
COMPARISON OF THE RESULTS

	Conventional Method		Proposed Method	
Sensor position	Inductor		Load	
Current feedback	Sensor feedback		Observer feedback, Sensor feedforward	
	Thyristor rectifier	Diode rectifier	Thyristor rectifier	Diode rectifier
V_o at 60Hz	192.7 V	194.8 V	192.9 V	192.9 V
V_o at 180Hz	6.8 V	9.72 V	0.45 V	3.54 V
V_o at 300Hz	3.75 V	6.52 V	2.91 V	1.53 V
V_o at 420Hz	5.1 V	1.99 V	1.97 V	1.06 V
V_o at 540Hz	3.92 V	0.68 V	1.78 V	1.05 V
V_o THD	**6.2 %**	**6.14 %**	**2.35 %**	**2.2 %**

ACKNOWLEDGMENT

This work was supported by the Korea Institute of Energy Technology Evaluation and Planning(KETEP) and the Ministry of Trade, Industry & Energy(MOTIE) of the Republic of Korea (No. 20162220200010).

REFERENCES

[1] S. Buso, S. Fasolo, and P. Mattavelli, "Uninterruptible power supply multiloop control employing digital predictive voltage and current regulators," *IEEE Trans. Ind. Appl*., Vol. 37, No. 6, pp. 1846-1854, Nov./Dec. 2001.

[2] P. Mattavelli, F. Polo, F. D. Lago, and S. Saggini, "Analysis of control-delay reduction for the improvement of UPS voltage-loop bandwidth," *IEEE Trans. Ind. Electron.*, Vol. 55, No. 8, pp. 2903-2911, Aug. 2008.

[3] N. D. T. Yokoyama, and T. Ishioka, "Verification of an autonomous decentralized UPS system with fast transient response using a FPGA-based hardware controller," *Journal of Power Electronics*, Vol. 9, No. 3, pp. 507-515, May 2009.

[4] S. Karve, "Three of a kind [UPS topologies, IEC standard]," *IEE Review*, Vol. 46, No. 2, pp. 27-31, Mar. 2000.

[5] J. M. Choe, B. J. Byen, S. Moon, and J. S. Lai, "A capacitor current control for stand-alone inverters using an inductor current observer," in *9th International Conference on Power Electronics and ECCE Asia (ICPE-ECCE Asia)*, pp. 1143-1148, Jun. 2015.

[6] N. M. Abdel-Rahim and J. E. Quaicoe, "Analysis and design of a multiple feedback loop control strategy for single-phase voltage-source UPS inverters," *IEEE Trans. Power Electron.*, Vol. 11, No. 4, pp. 532-541, Jul. 1996.

[7] M. J. Ryan, W. E. Brumsickle, and R. D. Lorenz, "Control topology options for single-phase UPS inverters," *IEEE Trans. Ind. Appl.*, Vol. 33, No. 2, pp. 493-501, Mar./Apr. 1997.

[8] J. Rodriguez, J. Pontt, C. A. Silva, P. Correa, P. Lezana, P. Cortes, and U. Ammann, "Predictive current control of a voltage source inverter," *IEEE Trans. Ind. Electron.*, Vol. 54, No. 1, pp. 495-503, Feb. 2007.

[9] J. S. Cho, S. Y. Lee, H. S. Mok, and G. H. Choe, "Analysis and design of modified deadbeat controller for 3-phase uninterruptible power supply," in *Proceedings of the IEEE 1999 International Conference on Power Electronics and Drive Systems (PEDS)*, Vol. 2, pp. 1003-1009, Jul. 1999.

[10] P. Mattavelli, "An improved deadbeat control for UPS using disturbance observers," *IEEE Trans. Ind. Electron.*, Vol. 52, No. 1, pp. 206-212, Feb. 2005.

[11] S. Buso, S. Fasolo, L. Malesani, and P. Mattavelli, "A dead-beat adaptive hysteresis current control," *IEEE Trans. Ind. Appl.*, Vol. 36, No. 4, pp. 1174-1180, Jul./Aug. 2000.

[12] G. Escobar, A. A. Valdez, J. Leyva-Ramos, and P. Mattavelli, "Repetitive-based controller for a UPS inverter to compensate unbalance and harmonic distortion," *IEEE Trans. Ind. Electron*., Vol. 54, No. 1, pp. 504-510, Feb. 2007.

[13] P. C. Loh, M. J. Newman, D. N. Zmood, and D. G. Holmes, "A comparative analysis of multiloop voltage regulation strategies for single and three-phase UPS systems," *IEEE Trans. Power Electron.*, Vol. 18, No. 5, pp. 1176-1185, Sep. 2003.

[14] P. C. Loh and D. G. Holmes, "Analysis of multiloop control strategies for LC/CL/LCL-filtered voltage-source and current-source inverters," *IEEE Trans. Ind. Appl.*, Vol. 41, No. 2, pp. 644-654, Mar./Apr. 2005.

[15] M. Monfared, S. Golestan, and J. M. Guerrero, "Analysis, design, and experimental verification of a synchronous reference frame voltage control for single-phase inverters," *IEEE Trans. Ind. Electron.*, Vol. 61, No. 1, pp. 258-269, Jan. 2014.

[16] J. He and Y. W. Li, "Generalized closed-loop control schemes with embedded virtual impedances for voltage source converters with LC or LCL filters," *IEEE Trans. Power Electron.*, Vol. 27, No. 4, pp. 1850-1861, Apr. 2012.

[17] Y. A. R. I. Mohamed, "Mitigation of dynamic, unbalanced, and harmonic voltage disturbances using grid-connected inverters with LCL filter," *IEEE Trans. Ind. Electron*., Vol. 58, No. 9, pp. 3914-3924, Sep. 2011.

[18] Q. Lei, F. Z. Peng, and S. Yang, "Multiloop control method for high-performance microgrid inverter through load voltage and current decoupling with only output voltage feedback," *IEEE Trans. Power Electron*., Vol. 26, No. 3, pp. 953-960, Mar. 2011.

[19] D. Dong, T. Thacker, R. Burgos, F. Wang, and D. Boroyevich, "On zero steady-state error voltage control of single-phase PWM inverters with different load types," *IEEE Trans. Power Electron.*, Vol. 26, No. 11, pp. 3285-3297, Nov. 2011.

[20] G. Escobar, P. Mattavelli, A. M. Stankovic, A. A. Valdez, and J. Leyva-Ramos, "An adaptive control for UPS to compensate unbalance and harmonic distortion using a combined capacitor/load current sensing," *IEEE Trans. Ind. Electron.*, Vol. 54, No. 2, pp. 839-847, Apr. 2007.

[21] M. J. Ryan and R. D. Lorenz, "A high performance sine wave inverter controller with capacitor current feedback and “back-EMF” decoupling," in *26th Annual IEEE Power Electronics Specialists Conference (PESC)*, Vol. 1, pp. 507-513, Jun. 1995.

[22] D. G. Luenberger, "An introduction to observers," *IEEE Trans. Autom. Control*, Vol. 16, No. 6, pp. 596-602, Dec. 1971.

[23] H. D. Venable, "The k-factor: a new mathematical tool for stability analysis and synthesis," in *POWERCON*, pp. 1-12, 1983.

[24] J. S. Lai, "ECE6204 lecture note," ed, pp. 11.23 - 11.26, 2015.

Jung-Muk Choe received his B.S., M.S. and Ph.D. degrees in Electrical Engineering from Konkuk University, Seoul, Korea, in 2008, 2010 and 2014, respectively. From 2010 to 2011, he was a researcher for LSIS, Korea. He is presently a Postdoctoral Researcher at the Virginia Polytechnic Institute and State University (Virginia Tech), Blacksburg, VA, USA. He received a Contribution Award from the *Journal of Power Electronics*, a Contribution Award and an Academic Award from Konkuk University. His current research interests include the design of high power converters.

Seungryul Moon was born in Korea, in 1981. He received his M.S. and Ph.D. degrees in Electrical Engineering from the Virginia Polytechnic Institute and State University (Virginia Tech), Blacksburg, VA, USA, in 2007 and 2017, respectively. He was with the Transverse Flux Machine Research Group, Korea Electrotechnology Research Institute (KERI), Changwon, Korea, from 2007 to 2011. His current research interests include the design of power converters and motor drivers.

Byeng-Joo Byen received his B.S. and M.S. degrees from Konkuk University, Seoul, Korea, in 2011 and 2013, respectively, where he is presently working towards his Ph.D. degree in Power Electronics. His current research interests include electric vehicle chargers and single-phase inverter control methods.

Jih-Sheng Lai received his M.S. and Ph.D. degrees in Electrical Engineering from the University of Tennessee, Knoxville, TN, USA, in 1985 and 1989, respectively. In 1989, he joined the Electric Power Research Institute (EPRI) Power Electronics Applications Center (PEAC), where he managed EPRI-sponsored power electronics research projects. In 1993, he joined the Oak Ridge National Laboratory as the Power Electronics Lead Scientist, where he initiated a high power electronics program and developed several novel high power converters including multilevel converters and soft-switching inverters. In 1996, he joined the Virginia Polytechnic Institute and State University (Virginia Tech), Blacksburg, VA, USA. He is presently serving as the James S. Tucker Professor in the Electrical and Computer Engineering Department and as the Director of the Future Energy Electronics Center (FEEC). He also holds an Honorary International Chair Professorship at the National Taipei University of Technology, Taipei, Taiwan, and he serves as a Visiting Professor at Nanyang Technological University, Singapore. His current research interests include high efficiency power electronic conversions for high power and energy applications. He has published more than 370 referenced technical papers and 2 books. He has also received 25 U.S. patents. He received a Technical Achievement Award on Lockheed Martin Award Night, 2 Journal Paper Awards, 11 Best Paper Awards from IEEE sponsored conferences, and a Virginia Tech Dean's Award on Research Excellence. He led student teams to win Top Three Finalist in the Google Little Box Challenge in 2016, Grand Prize Award from the International Future Energy Challenge (IFEC) in 2011, and Grand Prize Award in the Texas Instruments' Engibous Analog Design Competition in 2009. Dr. Lai is the Founding Chair of the 2001 IEEE Future Energy Challenge (FEC) and the 2016 IEEE Asian Conference on Energy, Power, and Transportation Electrification (ACEPT). He is also the General Chair of the IEEE Workshop on Computers in Power Electronics (COMPEL 2000) and the IEEE Applied Power Electronics Conference and Exposition (APEC 2005). He was the recipient of a 2016 IEEE IAS Gerald Kliman Innovator Award.

Young-Bae Lim received his B.S. degree in Electrical Engineering from Wonkwang University, Iksan, Korea, in 1994; and his M.S. and Ph.D. degrees in Electrical Control Engineering from Hongik University, Seoul, Korea, in 1998 and 2007, respectively. From 1994 to 1996, he was a Researcher for Orientech, Korea. He is presently working as the Leader of the Convergence Research Team, Korea Electrical Safety Corporation, Korea. He is also the Secretary of the National Mirror Committee to the IEC TC72. His current research interests include the grounding of DC systems and safety in smart grid environments.

Gyu-Ha Choe received his B.S., M.S. and Ph.D. degrees from Seoul National University, Seoul, Korea, in 1978, 1980, and 1986, respectively. Since 1980 he has been with the Department of Electrical Engineering, Konkuk University, Seoul, Korea, where he is presently working as a Professor, and as the Chief Director of the Energy Electronics Research Center. Dr. Choe was the President (2007–2008) of the Korean Institute of Power Electronics (KIPE), Seoul, Korea. From 2012 to 2013, he was the Vice President of Konkuk University, Seoul, Korea. His current research interests include harmonic cancellation and active power filtering, pulse width-modulation control and PCS design for various static power converters including new and renewable energy sources such as photovoltaic generation and fuel-cell generation, technology related to DC distribution and EV charging, and fields related to electrical safety for power systems.